

Biochemistry. Author manuscript; available in PMC 2010 January 27.

Published in final edited form as:

Biochemistry. 2009 January 27; 48(3): 549–557. doi:10.1021/bi8020197.

# Disorder and Structure in the Rab11 Binding Domain of Rab11-Family Interacting Protein 2,†,‡

Jie Wei, Yuqi Liu, Kakoli Bose<sup>§</sup>, Gillian D. Henry, and James D. Baleja<sup>\*</sup>
Department of Biochemistry, Tufts University School of Medicine, Boston, MA 02111

#### **Abstract**

Rab11 plays a central role in plasma membrane recycling which returns cellular receptors for re-use at the cell surface. A recently identified family of Rab11 interacting proteins (FIP) includes FIP2. The C-terminal region of FIP2 is essential for colocalization with Rab11 on early endosomes and to enable formation of higher order oligomers. Rab11 binding and oligomerization of FIP2 are separable. Here we have determined the three-dimensional structure of the 40 residue coiled-coil oligomerization domain of FIP2 in the absence of Rab11 using NMR methods. The N-terminal half showed strong NOE cross-peaks and well dispersed NMR resonances, whereas the C-terminal half had fewer NOE cross-peaks and less chemical shift dispersion. The C-terminal 10 residues were mostly disordered. The final structures of the dimer had favorable Ramachandran angles and a rootmean-square deviation of  $0.59 \pm 0.13$  Å over superimposed backbone residues. The structure allows a comparison to a structure of FIP2 in complex with Rab11 that was determined crystallographically. In complex with Rab11, the C-terminal residues are not disordered, but have a helical structure that predicts residual dipolar coupling constants that are incompatible with those measured on the unbound FIP2. In both structures, a histidine residue is found at the normally hydrophobic position of the heptad repeat of the coiled-coil and here we show its ionization destabilizes the coiled-coil structure. Together these data allow us to build a model in which the binding of FIP-family proteins to Rab11 can be described in terms of conformational changes and that suggests new modes of regulation.

Eukaryotic cells internalize nutrients, fluids, and other molecules from the extracellular environment through the plasma membrane via a process called endocytosis. The Rab protein family members regulate vesicle tethering and docking with target membranes and ensure the precision of vesicle fusion. In particular, Rab11 plays a central role in plasma membrane recycling which returns cellular receptors for re-use at the surface (1,2).

Rab11 conducts its biological effects through interacting with effector proteins in a GTP-dependent manner. Rab11 behaves as a typical GTPase protein in which the GTP bound form is active and the GDP bound form is inactive. These two forms have different conformations in their switch 1 and switch 2 regions that are built on a scaffold of a central six-stranded  $\beta$  sheet flanked by two  $\alpha$  helices on each side (3). The interacting region of the effector is generally

<sup>&</sup>lt;sup>†</sup>Supported in part by NIH grant GM067985

<sup>‡</sup>Atomic coordinates have been deposited with the Research Collaboratory for Structural Bioinformatics Protein Databank, filename 2K6S and NMR assignments have been deposited at the BioMagResBank (BMRB) NMR structural database, accession number 15880.

<sup>\*</sup>To whom correspondence should be addressed at the Department of Biochemistry, 136 Harrison Avenue, Tufts University School of Medicine, Boston, MA 02111. Phone: (617) 636–6872. FAX: (617) 636–2409. E mail: jim.baleja@tufts.edu. \$Current address: ACTREC, KS-138, Plot 1 & 2, Sector 22, Kharghar, Navi Mumbai 410210, India

**SUPPORTING INFORMATION AVAILABLE** One table summarizing NMR chemical shift data and three figures of <sup>15</sup>N relaxation data, analysis of chemical shifts, and comparison of structures. This material is available free of charge via the Internet at http://pubs.acs.org.

a dimer of  $\alpha$ -helices arranged in a coiled-coil (4-6) although sometimes a helix is used to form a binding surface, but with structures different from a coiled-coil (7-9).

A recently identified family of Rab11 interacting proteins (FIP) includes six members to date: Rab11-FIP1 (FIP1) (10), Rab11-FIP2 (FIP2) (10), Rab11-FIP3 (FIP3/eferin) (10), Rab11-FIP4 (FIP4) (11), Rip11/FIP5 (12), and Rab Coupling Protein (RCP) (13). The FIP proteins share a highly homologous Rab11-binding domain at their C-termini, which overlaps a conserved region that mediates coiled-coil formation (Figure 1). FIP2 is perhaps the most extensively studied of the FIP proteins, and has distinct biological roles. FIP2 is unique in that it contains multiple (three) Asn-Pro-Phe (NPF) sequences that bind the EH domain of Reps1 thereby coordinating EGF-receptor signaling (14). Rab11-FIP2 also coordinates functions of Rab11 with myosin Vb (15). The C-terminal region of FIP2 was found to be essential for its colocalization with Rab11 on early endosomes and enables FIP2 to form higher order oligomers (14). For recycling of the transferrin receptor, expression of the C-terminal region of FIP2 induced aberrant tubulation of the compartment containing transferrin receptors, which could not be reversed by over-expression of Rab11, thus underlining the importance of the C-terminal region of FIP2 in receptor recycling (16).

Our previous study of FIP2 defined the boundaries of the Rab11 FIP Homology domain (RH domain) and found a 50 residue segment (RH50) that formed a coiled-coil and was able to bind Rab11 efficiently (Figure 1A). We showed that a preformed helical conformation was not necessary as constructs that showed little coiled-coil formation still interacted with Rab11 efficiently, and conversely a construct, RHCC, that had as much helical structure as RH50, did not bind Rab11. Limited proteolysis of RH50 showed that the C-terminal 10 residues were susceptible to cleavage and probably relatively disordered. These data are consistent with mutagenesis data on FIP2 that suggest Rab11 binding and oligomerization are separable, thus potentially representing distinct mechanisms of regulation in a cellular context (14).

The crystal structure of FIP2 in complex with Rab11 was determined while this work on FIP2 in the absence of Rab11 was in progress (9). Although the crystal was formed with a longer construct containing the last 100 residues of FIP2, the residues showing electron density (S450 to V498) were nearly the same as in the proteolytically-derived fragment RH50 (Figure 1). The overall crystal structure is a heterotetramer with dyad symmetry arranged as a Rab11-(FIP2)<sub>2</sub>-Rab11 complex. Switch 1 of Rab11 is bound in a pocket between the two helices, while switch 2 remains flexible and is only peripherally associated with the effector. FIP2 forms an α-helical coiled-coil which has a Rab11 binding patch on equivalent and opposite sides close to the C-terminus. The C-terminal ten residues of FIP2 were distinctly not disordered, but have a structure that is presumably induced by interaction with Rab11 and comprises an extension of the coiled-coil by 3 residues, a turn, a 3<sub>10</sub> helix, a short β-strand, and a loop (9). At the interface, hydrogen bonds are observed between backbone atoms L496 and V498 of FIP2 and F48 of Rab11 as well as between R497 of FIP2 and T50 of Rab11 (9). We do not know to what extent the structure in the absence of Rab11 resembles that in complex with Rab11, and therefore we assessed the structures of the RH50 and RHCC using NMR methods. More important, a dynamic perspective of the interaction is described in which the disorder in the unbound FIP2 protein permeates from the C-terminus into the coiled-coil. Furthermore, a histidine residue is found at the hydrophobic 'd' position of the heptad repeat and we show that ionization of this histidine changes the FIP2 coiled-coil structure.

## **MATERIALS AND METHODS**

## Sample Preparation

The expression and purification of unlabeled RHCC and RH50 have been described in detail previously (17). Uniformly <sup>15</sup>N-labeled and <sup>13</sup>C-labeled domains were obtained by using M9

medium containing either 1 g/l <sup>15</sup>N-ammonium chloride or 2 g/l <sup>13</sup>C-glucose, respectively. To prepare samples selectively <sup>15</sup>N-labeled in particular amino acids, an M9 medium was used that lacked ammonium chloride and instead contained a mixture of unlabeled amino acids except for the appropriate <sup>15</sup>N-labeled amino acid (150 mg/l for leucine; 67 mg/l for lysine) (18). A construct with a mutation (H463A) was prepared by PCR methods and purified using the same procedure as for wild-type.

#### NMR spectroscopy

Samples consisted of 0.8–1.2 mM domain in 20 mM phosphate, pH 7.3. Unless otherwise stated, all experiments were performed at 298 K on a Bruker Avance-600 spectrometer. Resonance assignments and NOE analyses were performed on a <sup>15</sup>N, <sup>13</sup>C-labeled RHCC sample using a suite of gradient enhanced NMR experiments as described (19). The backbone was assigned using mostly HNCA (20), HNCO (20), HN(CA)CO (21), HN(CO)CA (22), CBCANH (22), and CBCA(CO)NH (20) data whereas the side chains were assigned using 3D HCCH-TOCSY. NOEs were detected in a 3D NOESY-HSQC (15N-separated) on a Bruker DMX 800 spectrometer for greater sensitivity at the higher field. <sup>1</sup>H-<sup>15</sup>N residual dipolar couplings were measured using 10 to 15 mg/mL of filamentous bacteriophage Pf1 as the alignment medium (23). To obtain unambiguous intermolecular NOEs, a 2D <sup>13</sup>Cfiltered, <sup>13</sup>C-selected NOESY spectrum was recorded on a sample comprising a mixture of 50% <sup>12</sup>C-labeled protein and 50% <sup>13</sup>C-labeled protein that was refolded from 4M urea (24). 2D spectra were also collected on RHCC in 100% D<sub>2</sub>O solution. <sup>15</sup>N T<sub>2</sub> and NOE experiments were performed at 15 °C on a Bruker Avance 600 MHz spectrometer (25.26). All data were processed with Bruker XWINNMR. SPARKY was used for resonance assignment and measurement of NOE cross-peak intensities (27).

#### **Conformational Data and Structure Calculations**

NOEs used in structure calculation were measured from a 2D NOESY spectrum collected in D<sub>2</sub>O and from a 3D <sup>1</sup>H-<sup>15</sup>N-NOESY HSOC spectrum in H<sub>2</sub>O using a mixing time of 100 ms. Backbone dihedral angle restraints were derived from the secondary structure of the protein and the backbone chemical shift analysis program TALOS (28). Structures were calculated using the CNS program (version 1.1) (29) as described (30). The same calculation procedure used for monomer and dimer structures, except the latter used non-crystallographic dimer symmetry restraints for residues Y453 to L485. The NOE/hydrogen bond and dihedral constraints used the default force constants (75 kcal/Å<sup>2</sup> and 400 kcal/deg<sup>2</sup>, respectively). The Erepel function was replaced by a Lennard-Jones potential during the final Powell minimization (30). Ten initial structures of the complex were calculated without the residual dipolar coupling restraints. Alignment tensor parameters (Da and R) were determined using PALES (31). The residual dipolar coupling restraints were incorporated into the final calculation with a force scale from 0.01 to 50 kcal/Hz<sup>2</sup> in Cartesian space. The resulting 30 structures were validated by PROCHECK (32). Structural statistics were performed with PROCHECK. Structures were drawn using Pymol (DeLano Scientific, Palo Alto, CA) and MOLMOL 2k.2 (33).

## **Circular Dichroism**

Far-UV CD spectra were obtained on a JASCO model 810 spectropolarimeter by averaging two scans with a step size of 0.5 nm using a cuvette with a path length of 0.1 cm. Spectra were baseline corrected by buffer subtraction. Peptide concentrations were determined by UV absorbance at 280 nm. The ellipticity at 222 nm was measured as a function of temperature for thermal denaturation studies.

## **Equilibrium Unfolding Studies**

Protein samples (5  $\mu$ M) and urea stock solutions (10 M) were prepared in acetate-phosphate buffer that was prepared by mixing 20 mM acetic acid, 200 mM NaCl, 1 mM DTT with 20 mM Na<sub>2</sub>HPO<sub>4</sub>, 200 mM NaCl, 1 mM DTT to the desired pH as described previously (34). Fluorescence emission scans were acquired between 290 and 350 nm using excitation at 280 nm using a Jobin-Yvon Fluorolog-3 fluorometer. The average emission wavelength  $\langle \lambda \rangle$  was determined for each fluorescence spectrum using equation 1:

$$\langle \lambda \rangle = \sum_{i=1}^{N} (I_i \lambda_i) / \sum_{i=1}^{N} (I_i)$$
(1)

where  $\langle \lambda \rangle$  = average emission wavelength and  $I_i$  is the emission at wavelength  $\lambda_i$  (35). Data were fit to a two-state dimer to monomer model as described by equation 2:

$$N_2 \stackrel{Keq}{\longleftrightarrow} 2U$$
 (2)

where the protein is assumed to be either in a native homodimeric state  $(N_2)$  or an unfolded monomeric state (U) as described earlier (34). Data were also fit to a two-state monomer to monomer model as described by equation 3:

$$N \stackrel{Keq}{\longleftrightarrow} U$$
 (3)

where the protein is assumed to be either in a native monomeric state (N) or an unfolded monomeric state (U) as described (36). G values were calculated as described previously (34).

## **RESULTS**

#### Three-Dimensional Structure Determination of RH domain

Various constructs representing regions at the C-terminal end of Rab11-FIP2 were previously assessed by limited proteolysis in the absence of Rab11 (17). The circular dichroism spectra of RHCC and RH50 were also found to be nearly identical, suggesting that they have the same helical structure except for the additional C-terminal residues of RH50 which are disordered (17). The similarity in structure is consistent with  $^{15}N^{-1}H$  correlation NMR spectra that show very similar resonance positions for the structured parts of the peptides (37). Because RHCC comprising residues 450 to 489 gave better quality NMR spectra, it was then used for further optimization and detailed structural analysis.

Raising the temperature from 25 °C to 37 °C gave spectra with slightly narrower linewidths, but fewer observable resonances in the  $^{1}$ H,  $^{15}$ N HSQC spectrum. To reduce hydrogen exchange, we lowered the pH from 7.4 to 6.8, but the protein precipitated. Altering the salt concentration and adding trifluoroethanol (TFE) did not produce significant improvement of the spectra quality. The best NMR spectra were obtained in 20 mM phosphate, pH 7.3 (Figure 2). Despite the optimization of the sample, resonance lines were broad with  $T_2$  values of about 35 msec (Figure 1S), while the  $T_2$  value in a similarly sized coiled-coil is about 75 msec (38). The shorter  $T_2$  indicates either aggregation or the presence of internal motion. Although the quality of NMR spectra did not substantially change using concentrations between 0.3 and 1.2 mM, a small degree of hexamer formation was noted in analytical ultracentrifugation experiments (17), suggesting that some broadening may be due to transient aggregation. The  $T_2$  values

and <sup>15</sup>N(39) NOE values were uniform across the RHCC sequence indicating that there was little internal motion on the microsecond time scale. At this point the exact origin of the line broadening was unknown, but it was clear that NMR resonance assignment and structure determination of RHCC was going to be more challenging than one would normally expect for a dimer of 40 amino acid residues (about MW 10000), but a great deal of effort was invested because of the importance of the structure. NMR spectra have been recorded for coiled coil domains of similar size, suggesting that axial asymmetry was not likely to be an impediment for structure determination (40-42).

To determine resonance assignments of RHCC, a variety of NMR spectra were collected on unlabeled,  $^{15}\text{N-labeled},\,^{15}\text{N-labeled},\,^{15}\text{N-labeled},\,^{13}\text{C-labeled},\,^{12}\text{C},\,^{13}\text{C-labeled}$  samples. The  $^{1}\text{H-}^{15}\text{N}$  HSQC of selectively lysine-labeled and selectively leucine labeled samples were also helpful (37). Missing resonances mostly belong to presumably less ordered residues at the N- and C-termini, although some resonances also could not be observed or resolved for several residues in the C-terminal half. The backbone assignments of N, NH, Ca, and Ha were 90% completed (Table 1S).

Previous CD analysis clearly showed that RHCC is an  $\alpha$ -helical protein (17). Consistent with the CD analysis, most of the H $\alpha$  chemical shifts of the amino acids showed an upfield shift with respect to the random coil values (Figure 3A), the C $\alpha$  chemical shifts showed downfield shifts and most C $\beta$  showed upfield shifts (Figure 2S), which reflect the helical configuration of the protein (43,44). In general the N-terminal half showed greater secondary shifts than the C-terminal half, suggesting stronger helix formation.

Backbone torsion angles of RHCC were predicted by TALOS (45) based on matching the  $C\alpha$ ,  $C\beta$ , N, and  $H\alpha$  chemical shifts of three consecutive residues to patterns observed in a database of proteins of known structure (45). NOE distance constraints and local dihedral angle measurements from TALOS were insufficient to derive satisfactory structures. Residual dipolar coupling (RDC) information proved to be very useful for deriving structures with acceptable precision.

The N-terminal (residue S450) and the C-terminal (residues L484 to M489) regions were poorly defined as few restraints per residue were observed. Elsewhere, one bond RDC's between amide hydrogens and amide nitrogens were similar with a value of about -19 Hz, consistent with the structure of a typical helix in which the amide nitrogen forms a hydrogen bond to the carbonyl of the i-4 residue such that the orientation of each N-H vector is the same and parallel to the long axis of the helix. Residues at a and d positions had slightly smaller RDC values (-23 to -24 Hz), consistent with observations made before on other coiled coils where the portion of the helix at the dimer interface is slightly compressed while those facing outside are stretched (46).

Structure calculation was initiated on the monomer starting from an extended chain conformation using CNS (29). A subset of 323 distance restraints was used for calculations that were then refined using RDC data (47). Excluding the N- and C-terminal regions, the root-mean-square-deviations of the 30 structures against their mean coordinates were 0.43 Å for backbone atoms and 1.16 Å for heavy atoms. Most  $\phi,\psi$  backbone torsion angles were within the allowed region of the Ramachandran plot (Table 1). The structure of RHCC reveals a slightly curved  $\alpha$ -helix from residue T452 to N483. The C terminal region from L484 to M489 was not well defined, as expected given the limited number of NOE restraints per residue. One possible explanation is that this region is not well structured, thus giving many fewer NOEs, which agrees with several unobservable resonances in this region and, for the resonances that could be seen, the approach to zero secondary chemical shifts. Because a limited proteolysis study using trypsin indicates that R487 is protected, suggesting that it lies in the structured core

(17), the structure N-terminal to this residue (probably N-terminal to N483) may block access by trypsin. The C-terminal region from L484 to M489 is important however for coiled-coil stability, as a peptide containing residues S450 to N483 lacked dispersion in its <sup>1</sup>H NMR spectrum and showed little CD signal at 222 nm indicative of helix formation (data not shown). L484 to M489 showed residual dipolar coupling constants that were about the same as the helical residues closer to the N-terminus. However, their secondary chemical shifts and NOE's typical of helical conformations were weaker, indicating formation of a transient helix. The line-widths of peaks in this region were slightly broader than elsewhere in the molecule.

A superposition of the mean structure of backbone of the monomer to the structure bound to Rab11 had a r.m.s. deviation of 0.98 Å (Figure 4B). The differences in side-chain conformations are not likely to be significant, because few stereospecific assignments or chi-1 angle determinations were made for the NMR structure and thus the side-chain conformations were under-determined. The slightly bent helix body is consistent with the super-coiled dimeric nature of the protein and with the crystal structure.

Only one set of NMR resonances corresponding to RHCC was observed, providing evidence that this dimer is symmetric. The most often violated NOE measurements during the calculation of the monomeric structure were centered on residues Y453, V456, L460, and H463. These NOEs were then re-introduced in the calculation as 18 inter-monomer restraints for violations larger than 2 Å and as 9 ambiguous restraints (intra- or inter-monomer) for violations smaller than 1 Å. These residues were also observed in the X-ray structure to be at the dimer interface. In addition, a few inter-chain NOEs primarily involving Y453 were obtained from <sup>12</sup>Cfiltered/13C-selected 3D NOESY designed to measure NOEs between one chain that was unlabeled and the other that was <sup>13</sup>C-labeled, although the signal-to-noise in this experiment was too low to be of much use. They were characteristic of side-chain packing of the residues in heptad repeats and consistent with the crystal structure. Structures of the dimer were calculated using a total of 1302 restraints, including 1081 NOEs, 153 dihedral restraints, and  $68 \, ^1J_{\mathrm{NH}}$  residual dipolar couplings. The final total energy was -116.4 kcal/mol and the backbone r.m.s. deviation of superimposed structures was  $0.59 \pm 0.13$  Å. Over 83% of residues had favored phi-psi torsion angles by PROCHECK analysis, and therefore the structure was of high quality (Table 1).

A ribbon diagram of a backbone superposition of 30 structures and a representative structure shows the expected coiled-coil structure in the N-terminal half of the molecule, but with fraying of the coiled-coiled structure in the C-terminal half (Figure 5). Analysis of the distance difference matrix of RHCC unbound and bound to Rab11 show that while the monomeric units have the same structure and the N-terminal halves of the dimers have the same structure while the C-terminal halves of the dimers have different structures (Figure 3S). Consistent with the weaker secondary chemical shifts, most of the differences arise from a lack of experimental data specifying the contacts between the helices because of increased motion in the C-terminal half. Consistent with the weaker secondary chemical shifts, most of the differences arise from a lack of experimental data specifying the contacts between the helices because of increased motion in the C-terminal half. Although the deviation in the C-terminal half can partially be explained by poor chemical shift dispersion and fewer NOE distance restraints, some of the differences in the structure (in the absence of Rab11) and the structure when bound to Rab11 are obvious from analysis of the RDC data (Figure 3B). For example, residues R487 and V488 have experimental RDC values that are near zero, consistent with averaging of the NH vector in solution, while the RDC values calculated from the X-ray structure are about -20 Hz, consistent with those residues being in an α-helix. The most striking finding was that the residues that directly contact Rab11 in the crystal structure correspond to those less defined in NMR structure. For example, Y480 and I481, which are highly conserved residues in RH domains that form an extended hydrophobic surface with Rab11 that is essential to stabilization

of the complex in X-ray structure (9), show fewer than 10 NOE crosspeaks per residue in NMR data. In addition, the side chain of Y480 makes a hydrogen bond with the backbone of V46 in Rab11. In the complex, the  $3_{10}$  helix and extended  $\beta$  sheet of FIP2 align with the  $\beta$ 2 strand of Rab11, with residues R487, P493, P499, and Y500 playing a role in stabilizing the conformation of FIP2 in this region (9). Thus the NMR structure of the unbound FIP2 and the X ray structure of FIP2 while bound to Rab11 are distinctly different.

#### Assessment of the role of a buried histidine in RHCC structure

During optimization of the conditions for NMR analysis, we discovered that pH values below 7 gave NMR spectra of poor dispersion and lower molar ellipticity values in CD spectra (Figure 6A). We attributed the acid destabilization to ionization of H463 found at the hydrophobic 'd' position of the heptad repeat of the coiled-coil. (The other histidine, H473, is at the 'g' position and is exposed to the solvent in both the NMR and X-ray structures.) The pKa for denaturation was found to be 5.9, consistent with the titration of a histidine residue, although the pKa was difficult to determine accurately because the intensity of CD spectra were not reproducible near pH 5.5, the calculated isoelectric point of the peptide. Although a peptide in which H463 was mutated to alanine showed substantially less molar ellipticity, this ellipticity was no longer pH sensitive (Figure 6B). (Likewise the intensities of CD spectra at pH values near the calculated pI of this peptide, 5.1, were also variable, mostly likely due to some degree of precipitation.) To examine the pH dependencies in a system that avoids the isoelectric point, equilibrium unfolding in urea was used at pH 7.5 and 4.0 and changes in tertiary structure were monitored by tyrosine fluorescence. The unfolding of the proteins was found to be reversible at both pH values (Figure 6C and D). The data could be fit with a model in which the native dimer unfolds into a monomeric unfolded state with a single transition (equation 2) and the thermodynamic parameters were obtained from the fits. At pH 7.5, the free energy of unfolding  $(\Delta G_{H2O})$  for RHCC was found to be 12.3  $\pm$  0.1 kcal/mole. The H463A mutant had a  $\Delta G_{H2O}$ of  $10.6 \pm 0.2$  kcal/mole, i.e., 1.7 kcal/mol less stable (Figure 6C). At pH 4.0, RHCC ( $\Delta G_{H2O}$ of 9.7  $\pm$  0.3 kcal/mole) was less stable than it was at pH 7.5, with a  $\Delta\Delta G$  of -2.6 kcal/mol. However at pH 4, the H463A mutant ( $\Delta G_{H2O}$  of 10.7  $\pm$  0.2 kcal/mole) was more stable than wild type RHCC by 1 kcal/mol (Figure 6D). The H463A was equally stable at pH 4.0 and 7.5  $(\Delta G_{H2O})$  of  $10.7 \pm 0.2$  versus  $10.6 \pm 0.2$  kcal/mole). The data thus demonstrate that H463 is important for acid-induced destabilization.

## DISCUSSION

The work presented in this paper is the first to investigate the structure and function of an effector protein, Rab11-FIP2, in the absence of its binding partner Rab11. Although the recently published crystal structure of the effector-Rab11 complex shows a clear picture of interactions after binding, it does not provide information on the structure before binding. Together these data allow a model in which the binding of FIP-family proteins to Rab11 can be described in terms of conformational changes. In the Rab11-FIP2 complex, ten residues near the C-terminal end of FIP2 form a structure comprising a turn, a 3<sub>10</sub> helix, and a β sheet. However in the NMR HSQC spectra of the corresponding RH50 construct of unbound FIP2, none of these ten residues was visible, indicating that they are much less ordered unbound than when in complex with Rab11. Our NMR structure was therefore focused on RHCC, a construct with nine residues fewer at the C-terminus than RH50 (Figure 1A). The results from NMR were consistent with previous results obtained using CD spectroscopy (17). Some degree of partial disorder extends further into the coiled-coil of RHCC, as some C-terminal residues, while helical, show poor chemical shift dispersion and are not well defined structurally. This partial disorder is consistent with their participation in interacting with Rab11 (Y480, I481, L485-M489). Based on CD data in which an induced α-helical structure was apparent on complex formation, we hypothesized that structure is induced upon Rab11 binding (17). Consistent with

this hypothesis, these two structures with and without Rab11 in the RHCC covered area suggest that the change does not result from conformational changes within Rab11 (48), but from extra helix formation within FIP2 associated with the disorder-to-order transition that is centered on the Rab11 binding domain region of FIP2.

The characterization of dynamics within FIP2 allows several possibilities for regulation of its biological function. One possibility is that levels of unbound protein could be controlled by proteolysis as the less-ordered C-terminal end can be cleaved by trypsin as well as an *E. coli* enzyme with chymotrypsin like activity (17). On the other hand, cellular localization away from cytosolic proteases or binding to other proteins may protect FIP2 *in vivo*. Another possibility is that the flexibility of FIP2 when unbound allows binding to other proteins thus altering function. For example, a P85 SH3 binding site is strongly predicted for residues Y500 to P502, which would not be accessible when bound to Rab11 (41). The dynamics may also allow different choices to be made more readily than if FIP2 were rigid by allowing the unbound protein to sample a larger conformational space. Such a model would allow one to predict that Rab11 proteins that are on different vesicles or membranes that are separated by various distances could be brought together by FIP2 on complex formation with Rab11.

The H463 buried at the RHCC dimer interface impacts the stability of RHCC, and may provide an additional mechanism to regulate FIP2 biological function. Buried polar residues in the hydrophobic interface of the coiled-coil proteins are typical as they are important for oligomeric specificity (49-51), chain orientation and the kinetics of unfolding (52). A neutral histidine 463 at the FIP2 dimer interface, at pH 7 or higher preserves the dimeric structure and allows a stable complex with Rab11, which may directly or indirectly mediate vesicle and target membrane fusion (53). At lower pH, the protonated histidine destabilizes the dimeric FIP2, and would be predicted to weaken the interaction with Rab11. The histidine-dependent dissociation of dimeric structures have been observed before in other kinds of structures, but we are unaware of ionization of histidines that de stabilize coiled-coil formation (54,55). Several physiological conditions are associated with cellular pH values below pH 7, including hypoxia and apoptosis, although it remains to be determined whether the function of FIP2 *in vivo* is pH dependent (56-58).

The structure of FIP2 and the changes in this structure upon Rab11 binding suggests molecular mechanisms underlying endocytic recycling pathways (Figure 7). The dimeric Rab11-FIP2 appears to act as a scaffold that brings several proteins involved in vesicle sorting in addition to the binding of Rab11 for vesicle recycling (Figure 7). N-terminal to the coiled-coil (residues 453-491) and Rab11-binding domain (residues 477-498) are three NPF sequences (residues 324–326, 406–408, and 440–442) that play a role in recruiting proteins with Eps15 homology domains, such as EHD1 (59) and Reps1 (14). In the case of Reps1, FIP2 coordinates intracellular trafficking of components of the Ras/Ral signal transduction pathway. The possibility of crosstalk between FIP signaling pathways has been suggested ever since the evidence for the existence of heterodimers of FIPs in cell culture was presented (11,60), yet only homo-oligomers of FIPs are detected in vitro (60). The other potential intermolecular binding sites are the myosin Vb-binding domain (residues 129-290) that links endosomes to the cytoskeleton and the C2 lipid binding domain (residues 1–129) that links to the plasma membrane thus regulates cytoskeletal delivery of vesicles to the plasma membrane. Changes in FIP2 structure upon Rab11 binding might change the interactions with other partners such as EHD/Reps1, Myosin Vb, and the plasma membrane subsequently regulating the pathways that they are involved in.

In conclusion, biophysical experiments, an NMR solution structure, and the crystal structure of the complex, have together provided a picture of structural and dynamic aspects of the interaction between Rab11 and FIP2. While these studies have furthered our understanding of

the molecular mechanisms behind Rab11 binding to FIP2, they also suggest that homologues in the FIP family will behave similarly and show disorder-to-order transitions upon binding Rab11.

## **Supplementary Material**

Refer to Web version on PubMed Central for supplementary material.

#### **ACKNOWLEDGMENT**

We thank Dr. James Sudmeier for help with setting up 3D NMR experiments.

#### Abbreviations

CD, circular dichroism; FIP2, Rab11 Functional Interacting Protein-2; HSQC, heteronuclear single quantum coherence; NOE, nuclear Overhauser effect; RBD, Rab11 binding domain; RHCC, coiled coil region of Rab11-FIP homology domain; RDC, ; R.m.s., root mean-square.

## References

- 1. Wang X, Kumar R, Navarre J, Casanova JE, Goldenring JR. Regulation of vesicle trafficking in madindarby canine kidney cells by Rab11a and Rab25. J. Biol. Chem 2000;275:29138–29146. [PubMed: 10869360]
- Wilcke M, Johannes L, Galli T, Mayau V, Goud B, Salamero J. Rab11 regulates the compartmentalization of early endosomes required for efficient transport from early endosomes to the trans-golgi network. J. Cell. Biol 2000;151:1207–1220. [PubMed: 11121436]
- 3. Vetter IR, Wittinghofer A. The guanine nucleotide-binding switch in three dimensions. Science 2001;294:1299–1304. [PubMed: 11701921]
- 4. Ostermeier C, Brunger AT. Structural basis of Rab effector specificity: crystal structure of the small G protein Rab3A complexed with the effector domain of rabphilin-3A. Cell 1999;96:363–374. [PubMed: 10025402]
- 5. Zhu G, Zhai P, Liu J, Terzyan S, Li G, Zhang XC. Structural basis of Rab5-Rabaptin5 interaction in endocytosis. Nat. Struct. Mol. Biol 2004;11:975–983. [PubMed: 15378032]
- Shiba T, Koga H, Shin HW, Kawasaki M, Kato R, Nakayama K, Wakatsuki S. Structural basis for Rab11-dependent membrane recruitment of a family of Rab11-interacting protein 3 (FIP3)/ Arfophilin-1. Proc. Natl Acad. Sci. U S A 2006;103:15416–15421. [PubMed: 17030804]
- 7. Wu M, Wang T, Loh E, Hong W, Song H. Structural basis for recruitment of RILP by small GTPase Rab7. Embo J 2005;24:1491–1501. [PubMed: 15933719]
- 8. Eathiraj S, Pan X, Ritacco C, Lambright DG. Structural basis of family-wide Rab GTPase recognition by rabenosyn-5. Nature 2005;436:415–419. [PubMed: 16034420]
- Jagoe WN, Lindsay AJ, Read RJ, McCoy AJ, McCaffrey MW, Khan AR. Crystal structure of rab11 in complex with rab11 family interacting protein 2. Structure 2006;14:1273–1283. [PubMed: 16905101]
- Hales CM, Griner R, Hobdy-Henderson KC, Dorn MC, Hardy D, Kumar R, Navarre J, Chan EK, Lapierre LA, Goldenring JR. Identification and characterization of a family of Rab11-interacting proteins. J. Biol. Chem 2001;276:39067–39075. [PubMed: 11495908]
- 11. Wallace DM. The novel Rab11-FIP/Rip/RCP family of proteins displays extensive homo- and hetero-interacting abilities. Biochem. Biophys. Res. Commun 2002:909–915. [PubMed: 11944901]
- 12. Lindsay AJ, Hendrick AG, Cantalupo G, Senic-Matuglia F, Goud B, Bucci C, McCaffrey MW. Rab Coupling Protein (RCP), a novel Rab4 and Rab11 effector protein. J. Biol. Chem 2002;277:12190–12199. [PubMed: 11786538]
- 13. Prekeris R, Klumperman J, Scheller RH. A Rab11/Rip11 protein complex regulates apical membrane trafficking via recycling endosomes. Mol. Cell 2000;6:1437–1448. [PubMed: 11163216]

 Cullis DN, Philip B, Baleja JD, Feig LA. Rab11-FIP2, an adaptor protein connecting cellular components involved in internalization and recycling of epidermal growth factor receptors. J. Biol. Chem 2002;277:49158–49166. [PubMed: 12364336]

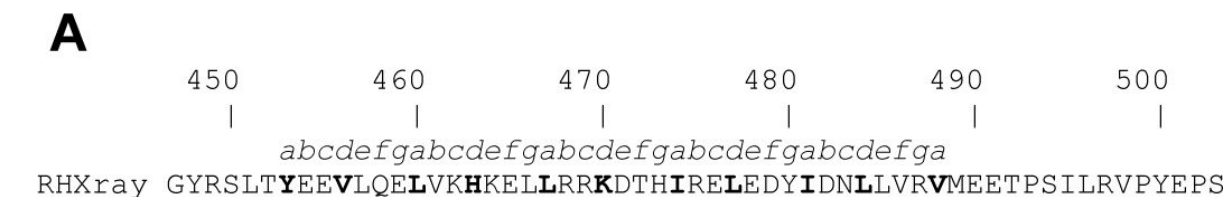
- Hales CM, Vaerman J-P, Goldenring JR. Rab11 Family Interacting Protein 2 associates with Myosin Vb and regulates plasma membrane recycling. J. Biol. Chem 2002;277:50415–50421. [PubMed: 12393859]
- Lindsay AJ, McCaffrey MW. Rab11-FIP2 functions in transferrin recycling and associates with endosomal membranes via its COOH-terminal domain. J. Biol. Chem 2002;277:27193–27199. [PubMed: 11994279]
- 17. Wei J, Fain S, Harrison C, Feig LA, Baleja JD. Molecular dissection of Rab11 binding from coiled-coil formation in the Rab11-FIP2 C-terminal domain. Biochemistry 2006;45:6826–6834. [PubMed: 16734419]
- 18. Griffey RH, Redfield AG, Loomis RE, Dahlquist FW. Nuclear magnetic resonance observation and dynamics of specific amide protons in T4 lysozyme. Biochemistry 1985;24:817–822. [PubMed: 3888265]
- 19. Alexander P, Faneshtock S, Lee T, Orban J, Bryan P. Thermodynamic analysis of the folding of streptococcal protein G IgG-binding domains B1 and B2: why small proteins tend to have high denaturation temperatures. Biochemistry 1992;31:3597–3603. [PubMed: 1567818]
- 20. Muhandiram DR, Kay LE. Gradient-Enhanced triple-resonance three-dimensional NMR experiments with improved sensitivity. Journal of Magnetic Resonance, Series B 1994;103:203–216.
- 21. Clubb RT, Wagner G. A triple-resonance pulse scheme for selectively correlating amide 1HN and 15N nuclei with the <sup>1</sup>H alpha proton of the preceding residue. J. Biomol. NMR 1992;2:389–394. [PubMed: 1324757]
- 22. Grzesiek S, Dobeli H, Gentz R, Garotta G, Labhardt AM, Bax A. <sup>1</sup>H, <sup>13</sup>C, and <sup>15</sup>N NMR backbone assignments and secondary structure of human interferon-gamma. Biochemistry 1992;31:8180–90. [PubMed: 1525157]
- 23. Hansen MR, Mueller L, Pardi A. Tunable alignment of macromolecules by filamentous phage yields dipolar coupling interactions. Nat. Struct. Biol 1998;5:1065–1074. [PubMed: 9846877]
- 24. Vuister GW, Kim S-J, Wu C, Bax A. 2D and 3D NMR study of phenylalanine residues in proteins by reverse isotopic labeling. J. Am. Chem. Soc 1994;116:9206–9210.
- 25. Kay LE, Torchia DA, Bax A. Backbone Dynamics of Proteins as studied by <sup>15</sup>N inverse detected heteronuclear NMR spectroscopy: Application to Staphylococcal nuclease. Biochemistry 1989;28:8972–8979. [PubMed: 2690953]
- 26. Dayie K, Wagner G. Relaxation-rate measurements for N-15-H-1 groups with pulse-field gradients and preservation of coherence pathways. Journal of Magnetic Resonance Series A 1995;111:121–
- 27. Agou F, Ye F, Goffinont S, Courtois G, Yamaoka S, Israel A, Veron M. NEMO trimerizes through its coiled-coil C-terminal domain. J. Biol. Chem 2002;277:17464–17475. [PubMed: 11877453]
- Al-Hashimi HM, Bolon PJ, Prestegard JH. Molecular symmetry as an aid to geometry determination in ligand protein complexes. Journal of Magnetic Resonance 2000;142:153–158. [PubMed: 10617446]
- 29. Brunger AT, Adams PD, Clore GM, DeLano WL, Gros P, Grosse-Kunstleve RW, Jiang JS, Kuszewski J, Nilges M, Pannu NS, Read RJ, Rice LM, Simonson T, Warren GL. Crystallography & NMR system: A new software suite for macromolecular structure determination. Acta Crystallogr D Biol Crystallogr 1998;54:905–921. [PubMed: 9757107]
- 30. Liu Y, Liu Z, Androphy E, Chen J, Baleja JD. Design and characterization of helical peptides that inhibit the E6 protein of papillomavirus. Biochemistry 2004;43:7421–7431. [PubMed: 15182185]
- 31. Zweckstetter M, Bax A. Prediction of sterically induced alignment in a dilute liquid crystalline phase: Aid to protein structure determination by NMR. J. Am. Chem. Soc 2000;122:3791–3792.
- 32. Laskowski RA, Rullmannn JA, MacArthur MW, Kaptein R, Thornton JM. AQUA and PROCHECK-NMR: programs for checking the quality of protein structures solved by NMR. J Biomol NMR 1996;8:477–486. [PubMed: 9008363]
- 33. Koradi R, Billeter M, Wuthrich K. MOLMOL: a program for display and analysis of macromolecular structures. J. Mol. Graph 1996;14:51–5. 29–32. [PubMed: 8744573]

34. Bose K, Yoder NC, Kumar K, Baleja JD. The role of conserved histidines in the structure and stability of human papillomavirus type 16 E2 DNA-binding domain. Biochemistry 2007;46:1402–11. [PubMed: 17260970]

- 35. Royer CA, Mann CJ, Matthews CR. Resolution of the fluorescence equilibrium unfolding profile of trp aporepressor using single tryptophan mutants. Protein Sci 1993;2:1844–1852. [PubMed: 8268795]
- 36. Santoro MM, Bolen DW. Unfolding free energy changes determined by the linear extrapolation method. 1. Unfolding of phenylmethanesulfonyl alpha-chymotrypsin using different denaturants. Biochemistry 1988;27:8063–8068. [PubMed: 3233195]
- 37. Wei, J. Ph. D. Thesis. Tufts University School of Medicine; Boston, MA: 2006. p. 185
- 38. MacKay JP, Shaw GL, King GF. Backbone dynamics of the c-Jun leucine zipper: <sup>15</sup>N NMR relaxation studies. Biochemistry 1996;35:4867–4877. [PubMed: 8664278]
- 39. Al-Hashimi HM, Pitt SW, Majumdar A, Xu W, Patel DJ. Mg<sup>2+</sup>-induced variations in the conformation and dynamics of HIV-1 TAR RNA probed using NMR residual dipolar couplings. J. Mol. Biol 2003;329:867–873. [PubMed: 12798678]
- 40. Greenfield NJ, Montelione GT, Farid RS, Hitchcock DeGregori SE. The structure of the N-terminus of striated muscle alpha tropomyosin in a chimeric peptide: nuclear magnetic resonance structure and circular dichroism studies. Biochemistry 1998;37:7834–7843. [PubMed: 9601044]
- 41. Gordon-Smith DJ, Carbajo RJ, Yang JC, Videler H, Runswick MJ, Walker JE, Neuhaus D. Solution structure of a C-terminal coiled-coil domain from bovine IF(1): the inhibitor protein of F(1) ATPase. J. Mol. Biol 2001;308:325–339. [PubMed: 11327770]
- 42. Walters KJ, Dayie KT, Reece RJ, Ptashne M, Wagner G. Structure and mobility of the PUT3 dimer. Nat. Struct. Biol 1997;4:744–750. [PubMed: 9303003]
- 43. Wishart DS, Sykes BD, Richards FM. The chemical shift index: a fast and simple method for the assignment of protein secondary structure through NMR spectroscopy. Biochemistry 1992;31:1647– 1651. [PubMed: 1737021]
- 44. Wishart DS, Sykes BD, Richards FM. Relationship between nuclear magnetic resonance chemical shift and protein secondary structure. J. Mol. Biol 1991;222:1423–1431.
- 45. Cornilescu G, Delaglio F, Bax A. Protein backbone angle restraints from searching a database for chemical shift and sequence homology. J. Biomol. NMR 1999;13:289–302. [PubMed: 10212987]
- 46. Mesleh MF, Veglia G, DeSilva TM, Marassi FM, Opella SJ. Dipolar waves as NMR maps of protein structure. J. Am. Chem. Soc 2002;124:4206–4207. [PubMed: 11960438]
- 47. Tjandra N, Omichinski JG, Gronenborn AM, Clore GM, Bax A. Use of dipolar <sup>1</sup>H-<sup>15</sup>N and <sup>1</sup>H-<sup>13</sup>C couplings in the structure determination of magnetically oriented macromolecules in solution. Nat. Struct. Biol 1997;4:732–738. [PubMed: 9303001]
- 48. Pasqualato S, Senic-Matuglia F, Renault L, Goud B, Salamero J, Cherfils J. The structural GDP/GTP cycle of Rab11 reveals a novel interface involved in the dynamics of recycling endosomes. J. Biol. Chem 2004;279:11480–11488. [PubMed: 14699104]
- 49. Hendsch ZS, Tidor B. Do salt bridges stabilize proteins? A continuum electrostatic analysis. Protein Sci 1994;3:211–226. [PubMed: 8003958]
- 50. Barlow DJ, Thornton JM. Ion-pairs in proteins. J. Mol. Biol 1983;168:867–885. [PubMed: 6887253]
- Rozwarski DA, Gronenborn AM, Clore GM, Bazan JF, Bohm A, Wlodawer A, Hatada M, Karplus PA. Structural comparisons among the short-chain helical cytokines. Structure 1994;2:159–173. [PubMed: 8069631]
- 52. Knappenberger JA, Smith JE, Thorpe SH, Zitzewitz JA, Matthews CR. A buried polar residue in the hydrophobic interface of the coiled-coil peptide, GCN4-p1, plays a thermodynamic, not a kinetic role in folding. J. Mol. Biol 2002;321:1–6. [PubMed: 12139928]
- 53. Akey DL, Malashkevich VN, Kim PS. Buried polar residues in coiled-coil interfaces. Biochemistry 2001;40:6352–6360. [PubMed: 11371197]
- 54. Cabezon E, Butler PJ, Runswick MJ, Walker JE. Modulation of the oligomerization state of the bovine F1-ATPase inhibitor protein, IF1, by pH. J. Biol. Chem 2000;275:25460–25464. [PubMed: 10831597]

55. Barbar E, Kleinman B, Imhoff D, Li M, Hays TS, Hare M. Dimerization and folding of LC8, a highly conserved light chain of cytoplasmic dynein. Biochemistry 2001;40:1596–1605. [PubMed: 11327818]

- 56. Shrode LD, Tapper H, Grinstein S. Role of intracellular pH in proliferation, transformation, and apoptosis. J. Bioenerg. Biomembr 1997;29:393–399. [PubMed: 9387100]
- 57. Gottlieb RA, Nordberg J, Skowronski E, Babior BM. Apoptosis induced in Jurkat cells by several agents is preceded by intracellular acidification. Proc. Natl Acad. Sci. U S A 1996;93:654–658. [PubMed: 8570610]
- 58. Xiong ZG, Chu XP, Simon RP. Ca<sup>2+</sup> -permeable acid-sensing ion channels and ischemic brain injury. J. Membr. Biol 2006;209:59–68. [PubMed: 16685601]
- 59. Naslavsky N, Rahajeng J, Sharma M, Jovic M, Caplan S. Interactions between EHD proteins and Rab11-FIP2: a role for EHD3 in early endosomal transport. Mol. Biol. Cell 2006;17:163–177. [PubMed: 16251358]
- 60. Junutula JR, Schonteich E, Wilson GM, Peden AA, Scheller RH, Prekeris R. Molecular characterization of Rab11 interactions with members of the family of Rab11-interacting proteins. J. Biol. Chem 2004;279:33430–33437. [PubMed: 15173169]
- 61. George M, Ying G, Rainey M, Solomon A, Parikh P, Gao Q, Band V, Band H. Shared as well as distinct roles of EHD proteins revealed by biochemical and functional comparisons in mammalian cells and C. elegans. BMC Cell Biology 2007;8:3. [PubMed: 17233914]



RH50 GSLTYEEVLQELVKHKELLRRKDTHIRELEDYIDNLLVRVMEETPSILRV

RHCC GSLTYEEVLQELVKHKELLRRKDTHIRELEDYIDNLLVRVM

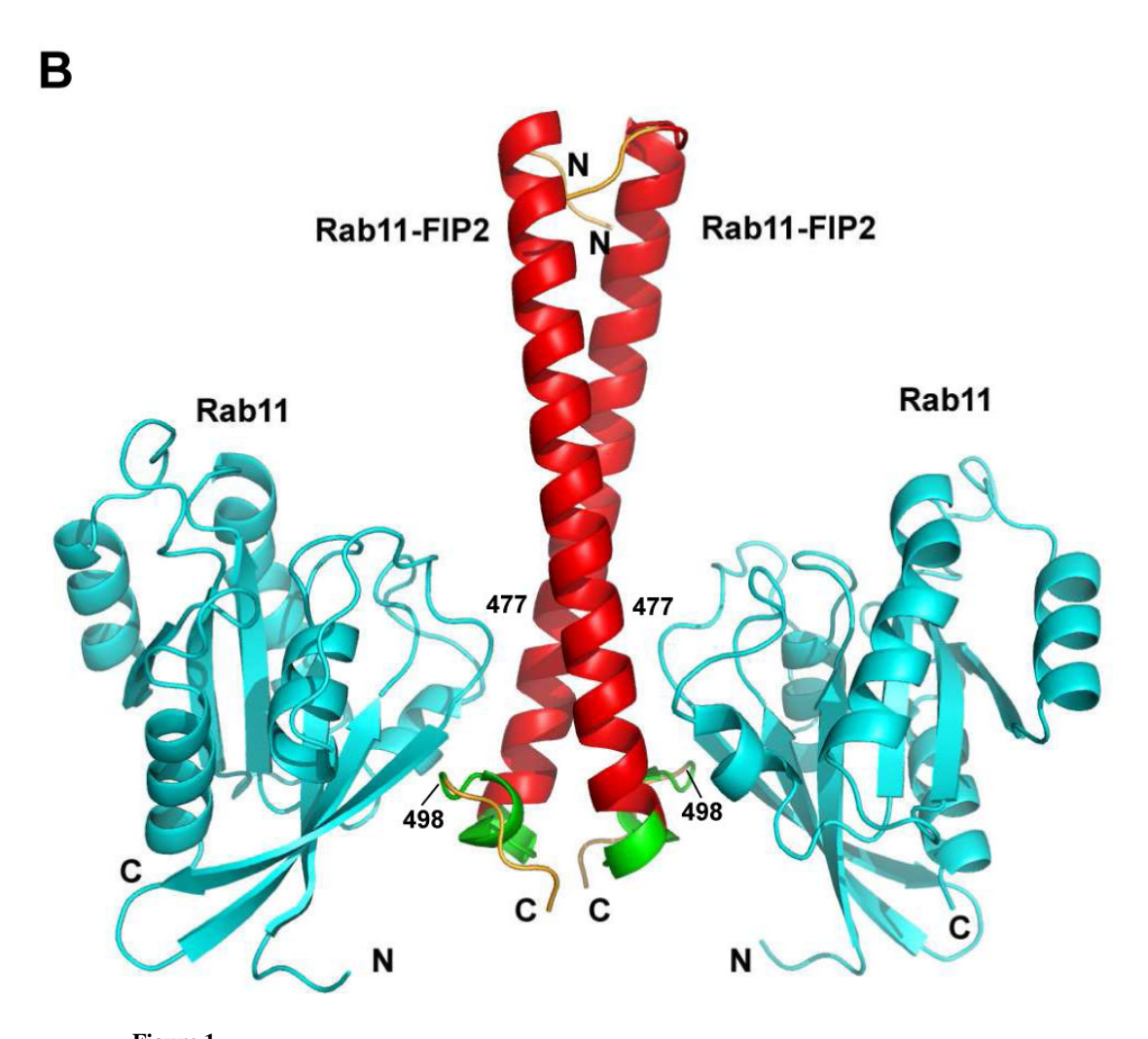


**Figure 1.**(A) Peptide sequences of Rab11-FIP2 containing the <u>Rab11-FIP Homology</u> domain. The X-ray structure of Rab11-FIP2 bound to Rab11 (9) showed electron density for residues 447 to 503 (RHXray). The italic letters above the sequences denote the predicted heptad repeats within the coiled-coil domain. Residues in the *a* and *d* positions are in bold and participate in the formation of a hydrophobic interface. The region of Rab11-FIP2 (residues 477–498) that interacts with Rab11 (RBD) is underlined. The 50 residue RH50 domain contains the minimal regions needed for both Rab11 binding and coiled coil formation, whereas the shorter RHCC domain contains the minimal region needed for coiled-coil formation (17). (B) Model of Rab11 in complex with Rab11-FIP2. The coordinates were from PDB entry 2GZH (9). The Rab11

molecules are shown in cyan. The RHCC portion of Rab11-FIP2 is shown in red and the portion unique to RH50 is shown in green. The boundaries (residues 477 and 498) of the Rab11-binding domain are indicated by residue numbers. Poorly structured residues at the N and C termini are in orange.

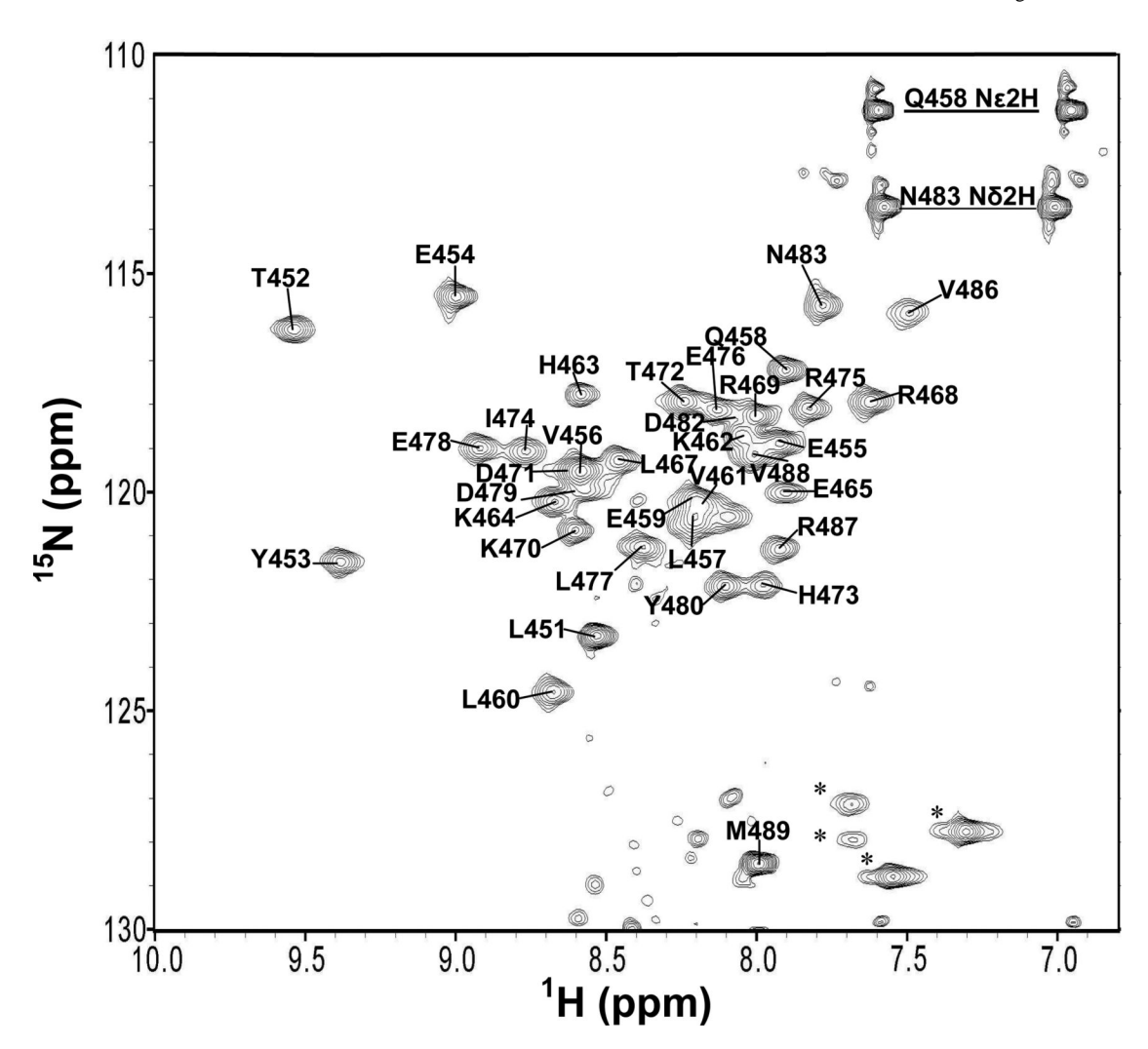
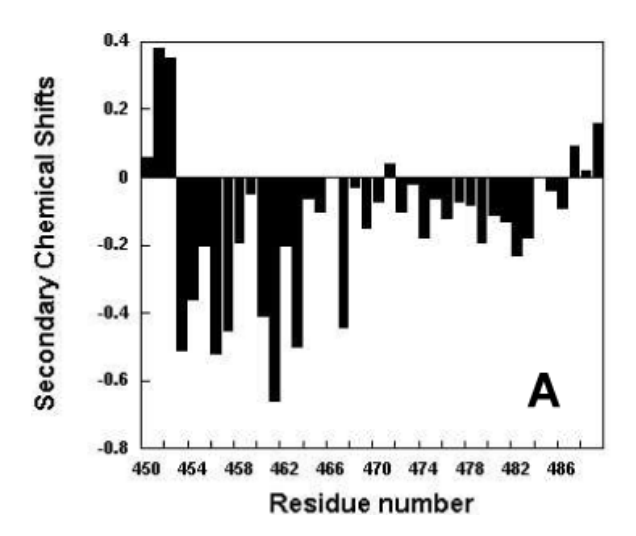


Figure 2. The 2D  $^{1}$ H, $^{15}$ N HSQC spectrum of uniformly  $^{15}$ N-labeled RHCC in 20 mM sodium phosphate buffer (pH 7.3) showing amide proton to nitrogen correlations that are labeled by residue number. Cross peaks for the side chain amides of asparagine and glutamine are joined by horizontal lines labeled with their assignments. Peaks labeled as \* correspond to the N $\epsilon$ H protons of the 4 arginine side chains. Unlabeled peaks are impurities due to small amount of degradation. The spectrum was collected at 600 MHz and 15  $^{\circ}$ C.



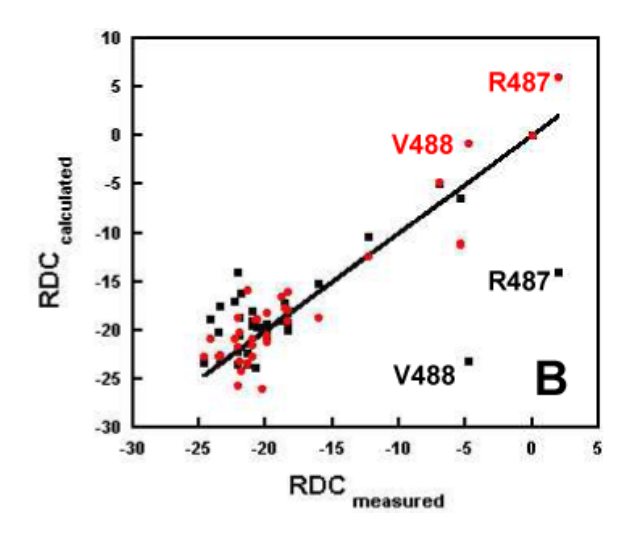
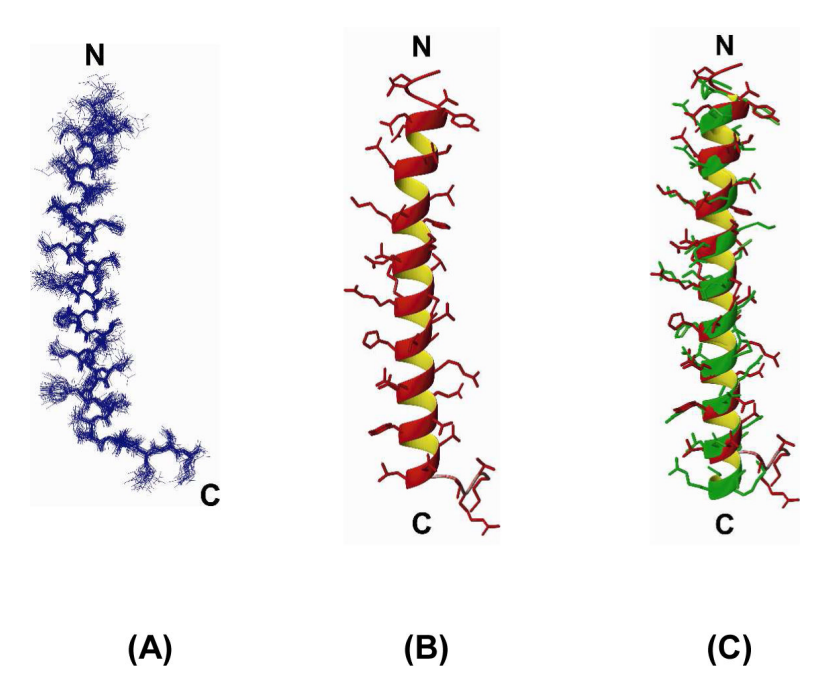
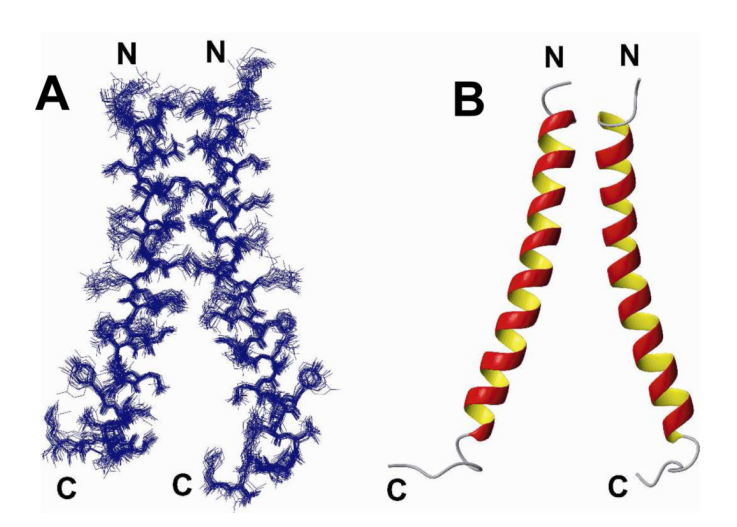


Figure 3. Structural assessment from chemical shifts and RDC data. (A) The H $\alpha$  chemical shifts of residues in RHCC were compared with the H $\alpha$  chemical shifts corresponding to a random coil conformation (secondary chemical shifts). (B) The fit of the experimental RDC data to that calculated from the X-ray model of RHCC (black squares) and NMR structure of RHCC (red circles). Two residues that fit the X-ray model poorly are labeled by residue number.



**Figure 4.**Three-dimensional structures of the monomer of RHCC. (A) Bundle of 30 superimposed in stereo (backbone atoms of Y453 to L384). (B) A representative structure. (C) Comparison of the monomer with the corresponding residues in the X-ray structure of the Rab11-FIP2/Rab11 complex. The NMR structure is in red and the X-ray structure is in green. The backbone r.m.s. deviation after superposition of residues C453 to L484 was 0.98 Å.



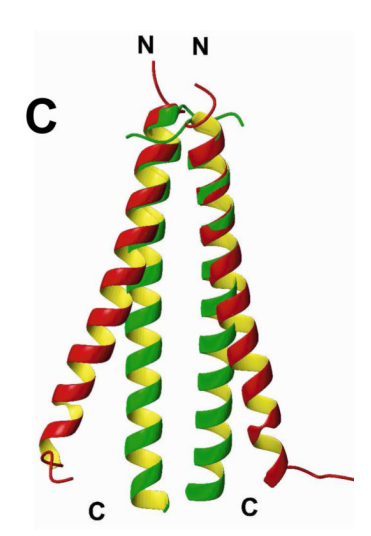


Figure 5.
Three-dimensional structures of the dimer of RHCC. (A) Bundle of 30 superimposed (backbone atoms of Y453 to L484). (B) A representative structure. (C) Comparison of a dimer of RHCC with the corresponding residues in the X-ray structure of the Rab11-FIP2/Rab11 complex. The NMR structure is in red whereas the X-ray structure is in green.

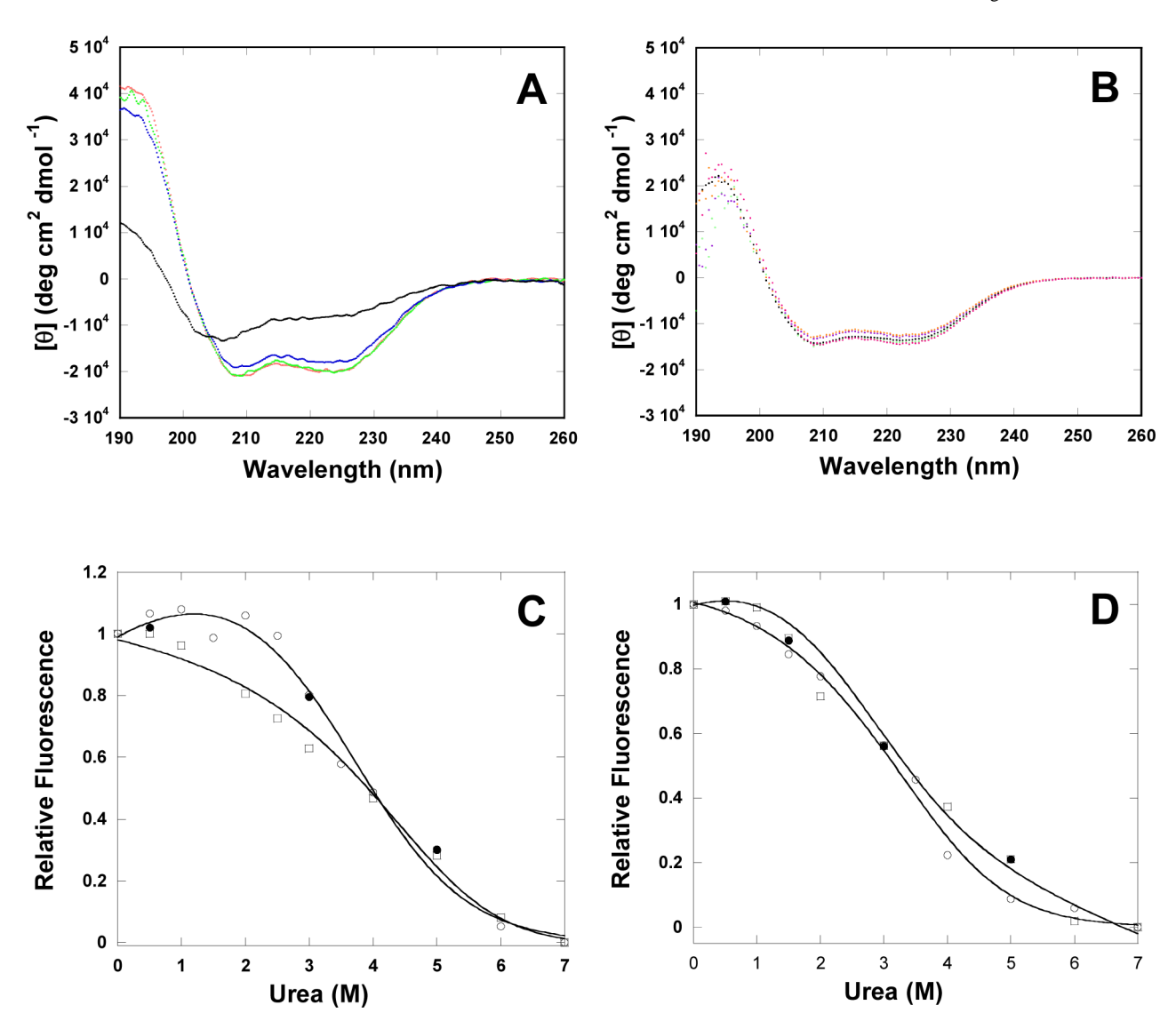


Figure 6. Stability of RHCC and its H463A mutant to pH and urea. (A) CD spectra of RHCC at pH 4.0 (black), 6.5 (blue), 7.0 (green), and 8.0 (red). (B) CD spectra of H463A at pH 3.3, 3.9, 6.3, 6.8, and 7.3. (C) Equilibrium unfolding data for RHCC ( $\circ$ ) and H463A ( $\square$ ) at pH 7.5. (D) Equilibrium unfolding data of RHCC ( $\circ$ ) and H463A ( $\square$ ) at pH 4.0. Corresponding refolding data are shown as closed symbols. Data were measured by recording the fluorescence average emission wavelength as a function of urea concentration. The protein concentrations were 5  $\mu$ M. Solid lines represent fits to the data using a dimer to monomer unfolding model that was used to derive the  $\Delta\Delta G_{H2O}$  values described in the text.

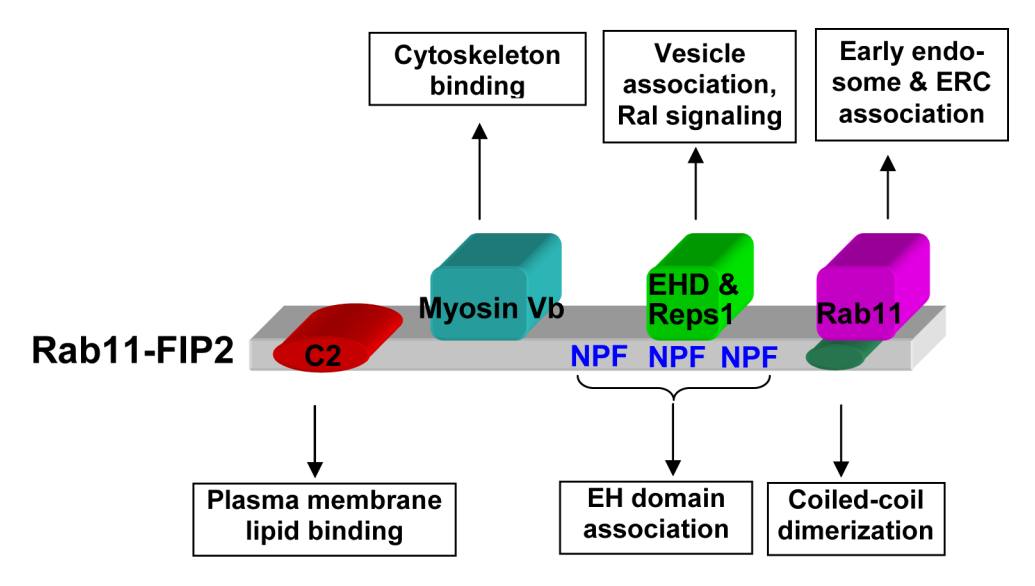


Figure 7.
Full length Rab11-FIP2 and its interacting proteins. The domain functions of Rab11-FIP2 are designated underneath the figure while sites of interactions with various proteins are above. C2 domains are typically associated with the membranes. Rab11-FIP2's NPF motifs are potential sites for binding EH domain-containing proteins. Two have been identified-EHD1, and close homologs, are associated with vesicular structures (61), while Reps1 binds RalBP1 as part of the Ral signaling cascade through Ras (14). In this paper, we determined the three-dimensional structure of RHCC, which represents the dimeric coiled-coil region. It partially overlaps with the Rab11 binding site. Rab11 is associated with the early endosome and plays a role in vesicle recycling.

Wei et al. Page 21

Table 1

NMR structural data and refinement statistics

	RH monomer	RH dimer
Number of experimental restraints		
Distance restraints from NOEs	323	1081
Dihedral angle restraints	78	153
RDC	30	68
Total No. of experimental restraints	431	1302
R.m.s. deviations from experimental data		
Average distance restraint violation (Å)	$0.008 \pm 0.002$	$0.007 \pm 0.001$
Distance restraint violations > 0.5 Å	$0.0\pm0.0$	$0.0\pm0.0$
Average dihedral angle restraint violation	$0.40\pm 0.11$	$0.68 \pm 0.19$
Dihedral angle restraint violations $> 5^{\circ}$	$0.0\pm0.0$	$0.0\pm0.0$
R.m.s. deviations from ideal stereochemistry		
Bonds (Å)	$0.0032 \pm 0.0001$	$0.0034 \pm 0.0001$
Angles (°)	0.41±0.03	$0.48 \pm 0.05$
Impropers (°)	0.37±0.06	$0.54 \pm 0.07$
Ramachandran analysis of the structures		
Residues in favored regions	90.9%	83.6%
Residues in additionally allowed regions	9.1%	16.3%
Residues in generously allowed regions	0.0%	0.1%
Residues in disallowed regions	0.0%	0.0%
Lennard-Jones potential energies		
Overall (kcal·mol <sup>-1</sup> )	$-96 \pm 18$	$-116 \pm 52$
Coordinate precision $(\mathring{\mathrm{A}})^a$		
Backbone	$0.43 \pm 0.11$	$0.59 \pm 0.13$
All heavy atoms	$1.16 \pm 0.14$	$1.16 \pm 0.16$

<sup>&</sup>lt;sup>a</sup>After superimposition of residues 453 to 484.